SANDIA REPORT

SAND2010-6504
Unlimited Release
September 2010

Chemical strategies for die/wafer sub-micron alignment and bonding

Lauren E. S. Rohwer, Alicia I. Baca, Dahwey Chu, James E. Martin

Prepared by
Sandia National Laboratories
Albuquerque, New Mexico 87185 and Livermore, California 94550

Sandia National Laboratories is a multi-program laboratory managed and operated by Sandia Corporation, a wholly owned subsidiary of Lockheed Martin Corporation, for the U.S. Department of Energy's National Nuclear Security Administration under contract DE-AC04-94AL85000.

Issued by Sandia National Laboratories, operated for the United States Department of Energy by Sandia Corporation.

Available to DOE and DOE contractors from
U.S. Department of Energy
Office of Scientific and Technical Information
P.O. Box 62
Oak Ridge, TN 37831

Telephone: (865) 576-8401
Facsimile: (865) 576-5728
E-Mail: reports@adonis.osti.gov
Online ordering: http://www.osti.gov/bridge

Available to the public from
U.S. Department of Commerce
National Technical Information Service
5285 Port Royal Rd.
Springfield, VA 22161

Telephone: (800) 553-6847
Facsimile: (703) 605-6900
E-Mail: orders@ntis.fedworld.gov
Online order: http://www.ntis.gov/help/ordermethods.asp?loc=7-4-0#online

SAND2010-6504
Unlimited Release
September 2010

Chemical strategies for die/wafer sub-micron alignment and bonding

Lauren E.S. Rohwer, Alicia I. Baca, Dahwey Chu
Advanced Microsystems Packaging

James E. Martin
Nanomaterials Sciences

Sandia National Laboratories
P.O. Box 5800
Albuquerque, New Mexico 87185-MS0892

Abstract

This late-start LDRD explores chemical strategies that will enable sub-micron alignment accuracy of dies and wafers by exploiting the interfacial energies of chemical ligands. We have micropatterned commensurate features, such as 2-d arrays of micron-sized gold lines on the die to be bonded. Each gold line is functionalized with alkanethiol ligands before the die are brought into contact. The ligand interfacial energy is minimized when the lines on the die are brought into registration, due to favorable interactions between the complementary ligand tails. After registration is achieved, standard bonding techniques are used to create precision permanent bonds. We have computed the alignment forces and torque between two surfaces patterned with arrays of lines or square pads to illustrate how best to maximize the tendency to align. We also discuss complex, aperiodic patterns such as rectilinear pad assemblies, concentric circles, and spirals that point the way towards extremely precise alignment.

ACKNOWLEDGMENTS

We thank the LDRD office and the Nanoscience to Microsystems Investment Area for providing the funding for this project. We would like to acknowledge Kevin Ewsuk, Wahid Hermina, Catalina Ahlers, Sharon Benson-Lucero, Javier Gallegos, Suzi Grine-Jones, Jeff Lantz, Jeremy Palmer, Terri Romanic, and Ben Thurston.

TABLE OF CONTENTS

FIGURES

TABLES

NOMENCLATURE

ENIG	Electroless nickel immersion gold
ENEPIG	Electroless nickel electroless palladium gold
MIL-STD	Military standard
SAM	Self-assembled monolayer
SNL	Sandia National Laboratories
XPS	X-ray photoelectron spectroscopy

1. INTRODUCTION

1.1. Background

It is currently only possible to align micropatterned features on die and wafers with those on other die and wafers with an accuracy of no better than ~5 microns, using the highest precision alignment equipment. To enable the integration of devices with ever-smaller feature sizes and increasing interconnect densities, sub-micron alignment is required.

There are surprisingly few papers on die/wafer alignment techniques. Capillary force alignment appears to be the most widely reported method [1-6]. Srinivasan et al. [1] used this approach to assemble microdevices patterned with square pads onto substrates with matching square pads, with an alignment accuracy of <0.2 μm. The gold on the microdevices and substrates are made hydrophobic with self-assembled monolayers (SAMs) of alkanethiols and an adhesive, respectively. The substrate is placed in a beaker of water and the microdevices are immersed in the water and directed to the substrate surface with a pipette. When the complementary hydrophobic patterns come into contact, the interfacial energy minimization of the adhesive-water and SAM-water interfaces leads to shape matching. The microdevices are held in place under water by the capillary forces of the adhesive. The final step in the process is to permanently bond the microdevices by curing the adhesive with UV light (for transparent substrates) and heat (for opaque substrates).

There has been some effort to develop a capillary-force-assisted alignment approach that does not involve adhesives. Water droplets that are confined within hydrophilic "cells" having hydrophobic gold borders have been used to align 2 inch glass wafers to 3 inch silicon wafers [2]. When wafers having complementary hydrophilic/hydrophobic cells are pressed together, the alignment is driven by the capillary forces of the water droplets. This method achieved an alignment accuracy of less than 1 μm. Tupek et al. [4] modeled this approach and determined the optimum number of droplets, and the effects of wafer bow on the alignment accuracy. Although submicron alignment is possible with this approach, the water trapped between the wafers is problematic for permanent bonding and for sensitive devices.

Alternative alignment methods have been proposed that are based on the surface tension of adhesives [7]; electrostatic forces [5]; and passive alignment based on the kinematic coupling and elastic averaging [8]. In Ref. 8, silicon wafers were KOH-etched with mating features

(pyramids and v-trenches). An alignment accuracy of 1 μm was achieved. However, the roughness of the etched surfaces prevents the use of silicon direct and anodic bonding. A new approach to the problem of aligning, then bonding devices is clearly needed.

1.2. Technical Approach

The ideal alignment method would be a dry method that does not require adhesives for permanent bonding. The method would be compatible with direct bonding techniques like SiO_2-SiO_2 and Au-Au and would achieve submicron alignment. A self-alignment process is amenable to these requirements. For instance, solder bump arrays have a self-aligning effect when a die and a substrate are bonded. Even if there is an initial misalignment, when the bumps reflow, the solder surface tension will cause the top die to shift into registry with the underlying wafer or substrate. Because solder bumps are too large to give sub-micron alignment, we turned to molecular self-assembled monolayers (SAMs) on patterned pads.

There are literally thousands of SAMs available, so we narrowed our selection to those that are compatible with gold and that can be used in our labs. This led us to alkanethiols ($CH_3(CH_2)_nSH$), since these bind strongly to gold. Alkanethiols have been used in several applications. The gold-patterned microdevices bonded to substrates in water, as previously described in the discussion of capillary force alignment, were coated with octadecanethiol [1]. Hexadecanethiol was shown to be an effective photoresist [9]. Dodecanethiol has been found to act as a lubricant and a passivation layer in Au-Au bonding studies [10,11] and as a corrosion barrier in Cu wire bonding studies [12]. In this LDRD we functionalized the gold features with dodecanethiol. X-ray photoelectron spectroscopy (XPS) studies have shown that Au surfaces coated with dodecanethiol SAMs have less oxygen and carbon contaminants than uncoated Au surfaces [10,12,13]. As a result, the surfaces can be bonded at lower temperatures and there are even reports of increased bond strength [10,11,14].

In the next section we discuss the theory behind our alignment concept. The ligand interactions must be combined with a pattern that maximizes the tendency of two surfaces to align.

1.2.1. Alignment force and torque

A computation of the alignment force and torque between two featured surfaces illustrates how best to pattern surfaces to maximize the tendency to align. We will start this discussion with the simple case of two surfaces patterned with lines, as in Figure 1. In this case these can be both a lateral and longitudinal force and a torque, and we will first compute the lateral force. Each surface is patterned with lines of width w with center-to-center separation d, and each line is of length L. The lines are comprised of material A, which in our experiments is Au that is sometimes coated with alkanethiols, and the gaps between the lines, of width (d-w), are material B, which we take as the underlying substrate, comprised of Pyrex or Si that may or may not be functionalized with a silane coupling agent. The interfacial energies per unit area will be denoted as γ_{ij}, where i and j denote materials A or B. These are the actual energies of these surfaces brought into contact, including any effect of asperities and other imperfections.

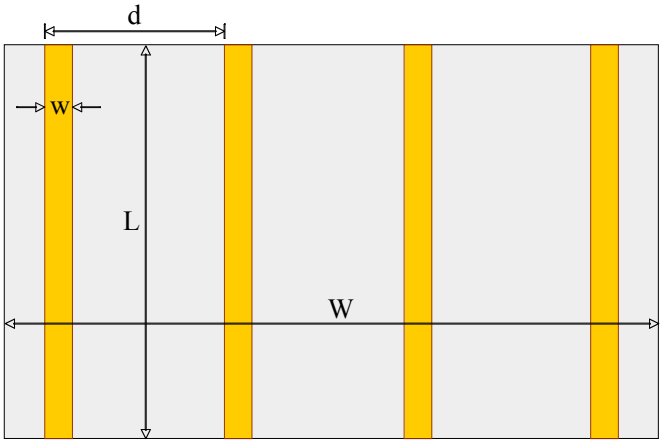

Figure 1. Patterning pattern intended to give alignment transverse to the lines.

Lateral force on an array of lines – In this case we assume the patterned lines are parallel and that the only misalignment is lateral to the lines, whose width $w \le d/2$. The variable x denotes the lateral displacement of the top surface relative to the bottom surface, which we take to be stationary, and $x=0$ corresponds to perfect alignment. For the case where $0 \le x \le w$, the interfacial energy per unit area of substrate is

$$\gamma = \frac{w-x}{d}\gamma_{\mathrm{AA}} + \frac{2x}{d}\gamma_{\mathrm{AB}} + \frac{d-w-x}{d}\gamma_{\mathrm{BB}}. \qquad (1)$$

Expressing the line width as $w=\alpha d$, where $\alpha \le 1/2$, gives

$$\gamma = \alpha\gamma_{AA} + (1-\alpha)\gamma_{BB} + \frac{x}{d}\Delta\gamma \qquad (2)$$

where the exchange energy per unit area is $\Delta\gamma = 2\gamma_{AB} - \gamma_{AA} - \gamma_{BB}$. The lateral *force per unit area f* is then just the negative spatial derivative of this areal energy,

$$f = -\frac{d\gamma}{dx} = -\Delta\gamma / d. \qquad (3)$$

For the lines to come into registration requires a negative force — which will occur for positive $\Delta\gamma$ — corresponding to those cases when materials A and B do not like to be in contact. Otherwise deregistration will be energetically favored. A plot of the surface energy and force are in Figure 2a. As a rough estimate of the areal force we can take the exchange areal energy to be 10 ergs/cm^2. For a line spacing of 20 microns the areal force is then just 5x10^3 dynes/cm^2. For a 1 cm^2 substrate the lateral force would be roughly that due to earth's gravity on a 5 g mass, which is clearly palpable.

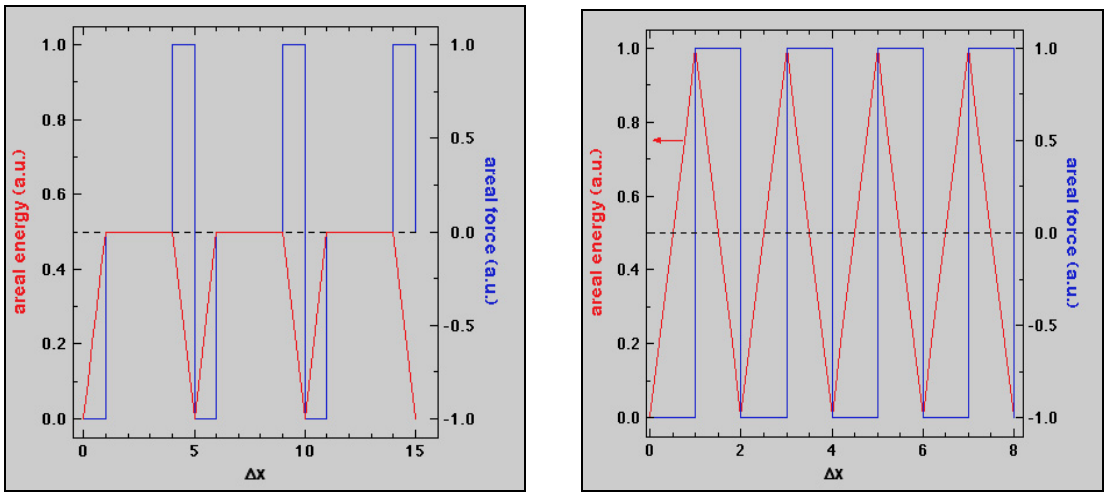

Figure 2. a) The registration surface energy and force as a function of lateral displacement. When there is no overlap between the material A lines (and therefore double overlap between the material B gaps between the lines) there is no force. b) In the case where the lines and spaces have the same width there are no force gaps of finite size.

A few aspects of Eq. 3 bear highlighting. First, the registration force is inversely proportional to the line spacing, but independent of the line width. Second, the areal force is an *intensive* property, being independent of the dimensions of the substrate, and because the areal static friction is also an intensive property, the ability of the registration force to ovecome static friction is independent of scale. Third, in the case where the lines of material A do not partially

overlap ($w<x<d-w$) the registration force will be zero. Avoiding this condition requires some care in the initial positioning of the top substrate, and this places an ultimate limitation of the periodicity of the lines. In the special case where the line width is just half the periodicity there is always a positive or negative force, Figure 2b, and this symmetric pattern gives the greatest tolerance of initial misregistration.

Longitudinal force on an array of lines – In this case the alignment force is due only to the edges of the substrate and is therefore extrinsic. For this reason we compute the *total* force F, not the areal force f. Let y denote the displacement parallel to the lines of the top substrate relative to the bottom substrate. The substrate is of size LxW, where L is the dimension parallel to the lines. The total surface energy Γ will be

$$\Gamma = (L-y)W\left\lfloor \frac{w}{d}\gamma_{AA} + \frac{d-w}{d}\gamma_{BB} \right\rfloor + 2yW\left\lfloor \frac{w}{d}\gamma_{A} + \frac{d-w}{d}\gamma_{B} \right\rfloor \qquad (4)$$

where γ_A and γ_B are the surface energies of materials A and B in contact with the surrounding atmosphere. Differentiating with respect to y gives the total force

$$F = W\left\lfloor \frac{w}{d}(2\gamma_A - \gamma_{AA}) + \frac{d-w}{d}(2\gamma_B - \gamma_{BB}) \right\rfloor \qquad (5)$$

It is important to note that this total longitudinal force depends only on the substrate width and is *independent* of the size scale of the features. Furthermore, this force scales as W, whereas the static friction scales as LxW, so this longitudinal force is negligible in a practical sense. Substantial lateral and longitudinal forces require pad assemblies.

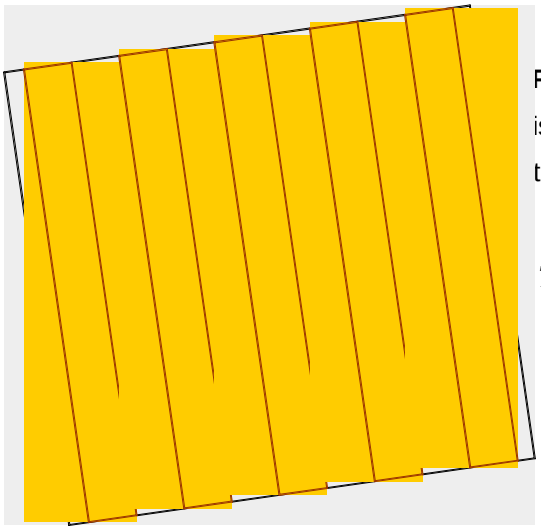

Figure 3. A series of lines misregistered by an angle θ that is small enough that the lines partially overlap throughout their length, creating a substantial alignment torque.

Torque on an array of lines – If there is angular

misalignment between the substrates then an aligning torque can result. This torque will be zero if the angular misalignment is large enough that each line crosses several other lines, but can be quite substantial if the misalignment is so small that each line overlaps with the underlying line to some extent throughout its entire length, as illustrated in Figure 3. For a substrate of width W containing lines of length L misaligned by a small angle θ the surface energy is

$$\begin{aligned}\Gamma &= \frac{W}{d}\frac{L^2}{2}\tan\theta\gamma_{AB} + \frac{W}{d}(wL - \frac{L^2}{4}\tan\theta)\gamma_{AA} + \frac{W}{d}\left((d-w)L - \frac{L^2}{4}\tan\theta\right)\gamma_{BB} \\ &= \frac{W}{d}\left[wL\gamma_{AA} + (d-w)L\gamma_{BB} + \frac{L^2}{4}\Delta\gamma\tan\theta\right].\end{aligned} \tag{6}$$

Differentiating this energy with respect to the angle θ gives the torque on the upper substrate

$$\mathrm{T} = -\frac{d\Gamma}{d\theta} \approx -A\frac{L}{4d}\Delta\gamma \tag{7}$$

where the A is the substrate area. This expression is correct to order θ and shows that the torque is similar to the lateral force in that it increases with decreasing feature size d and so can be quite substantial. Of course, the torque also scales with the line length. In the simple case of a square substrate, where L=W, the registration torque scales as L^3, and the static friction in rotation also scales like L^3, so the ratio of the registration torque to the static friction is scale independent, and therefore of practical importance.

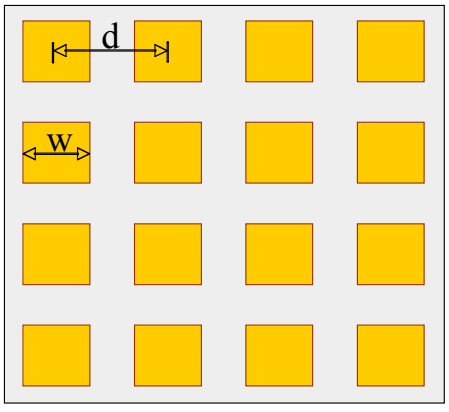

Figure 4. A square lattice of square pads.

Lateral and longitudinal force on a pad array -- The lateral and longitudinal areal force on a square lattice of square pads of size w with lattice spacing d, Figure 4, is easily obtained from Eq. 3. The pad array can be viewed as a series of dashed lines, so the lateral force is simply reduced from the expression in Eq. 3 by the factor w/d. The longitudinal areal force is clearly equal to this lateral areal force,

$$f = \frac{w}{d^2}\Delta\gamma \qquad (8)$$

For the reasonable case where $w = \frac{1}{2}d$ this areal force is just one half that obtained with lines.

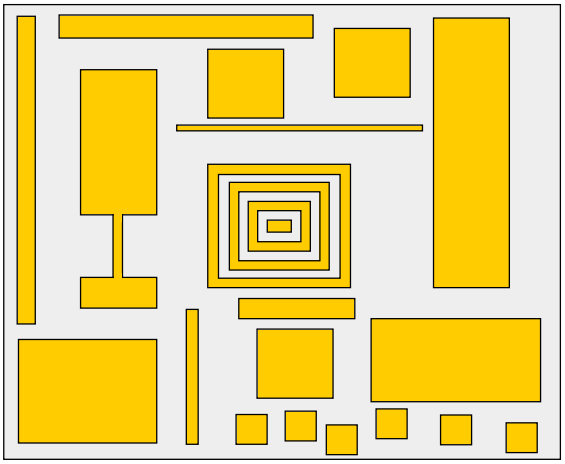

Figure 5. An arbitrary assembly of rectilinear pads.

Lateral and longitudinal force on an arbitrary assembly of rectilinear pads – The pad array result can be generalized to any assembly of rectilinear objects with their sides mutually aligned, Figure 5. Suppose we take as our Cartesian coordinates x,y and that the sides of these rectilinear pads are aligned with these axes. The *total* force F in the x direction will be one half the total length of the sides of all of the rectangles that are parallel to the y axis, times the exchange energy $\Delta\gamma$. That's the general result, and consistent with the fact that w/d^2 is just half the length of normal line *per unit area* for the square pad array. This result only applies when all of the mating features on each substrate are in close enough alignment that single feature overlap occurs everywhere. Such pad arrays point the way to extremely precise alignment: A succession of features of ever-decreasing size could lead to highly precise alignment given even a rough initial alignment. The ultimate precision would be limited only by the patterning precision.

More complex registration patterns – The periodic patterns we have analyzed above have the fault that the surface energy has many strong local minima (see Figure 2). Thus it is possible to have registration errors at integer multiples of the lattice periodicity. Simply increasing the line width is not a good approach, as the width of the potential wells scales with the line spacing, causing the registration force to decrease with increasing line width. It is better to create a pattern that maintains both the depth and width of the registration well of a fine line pattern, yet somehow increases the spacing between wells. To eliminate this problem one could use various

sorts of patterns that lack translational symmetry or have translational symmetry on a length scale large compared to the placement accuracy, and perhaps substantially larger than the line spacing. To illustrate this concept we consider the simple example of an array of lines with a sinusoidal modulation in their spacing.

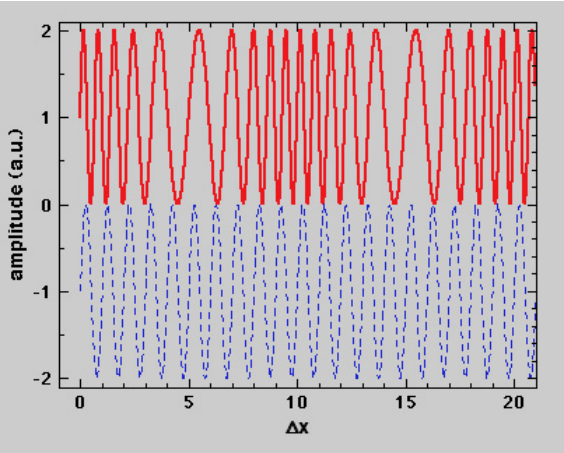

Figure 6. A phase-modulated surface composition fluctuation (solid line) is shown above a simple sinusoidal composition fluctuation with the same number of oscillations per unit length. The phase-modulated function has ten times the unit cell.

To simplify the computation of the interaction energy we consider a mathematical model that captures the *spirit* of this approach: a continuous composition modulation of the form $C(x) = \sin(2\pi kx + \phi(x))$, where $\phi(x) = A\sin(2\pi k' x)$. The 'potential surface' is then defined by the integral $U(\Delta x) = -\lim_{X\to\infty} \frac{1}{X}\int_0^X C(x)C(x+\Delta x)dx$. In Figure 6 we compare the unmodulated pattern (k=1, A=0) with the modulated pattern having k=1, k'=0.1, and A=5. In Figure 7 we give the potential surfaces for these two cases. The phase-modulated function increases the periodicity of the potential by a factor of k/k'=10, and decreases the amplitude of the minima in between the principal minima. Further increases in k/k' will increase the periodicity and greatly decrease the magnitude of the potential surface between the principal minima. This approach could greatly reduce the need for precision placement, while still retaining the high registration force given by fine lines. Alignment parallel to the lines could be achieved simply by making the lines wavy. These waves could also be phase modulated.

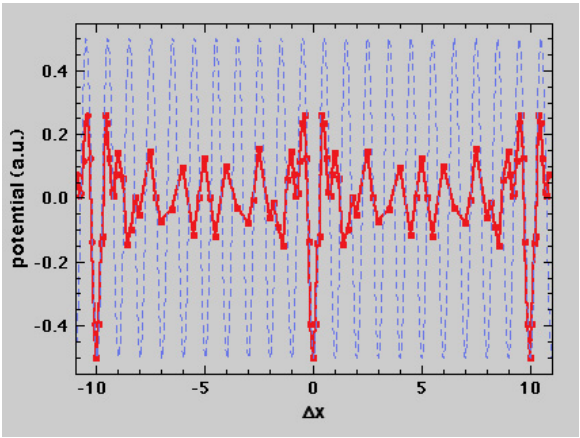

Figure 7. A comparison between the potential surfaces of the simple sinusoidal (dashed line) and phase-modulated composition fluctuations. If the phase-modulation wavevector is increased, the potential in between the principal minima is greatly reduced.

Many other approaches are possible. For example, Figure 8 shows the Moire pattern that occurs when two patterns of regularly spaced rings overlap. It is intuitively obvious that the surface energy is a weak function of the separation of the centers of these two patterns, until they come very close to concentricity. So one would expect a *single strong energy minimum*, and an associated radial force, to occur whose size is on the scale of the ring diameter, eliminating the possibility of misregistration. Of course, such a pattern would not generate a torque, but if two such patterns were on opposing corners of a die a large torque would occur. On the other hand, a single spiral pattern would generate both a radial force with a single minimum *and* a torque with a single minimum. Perhaps that is the optimal registration pattern.

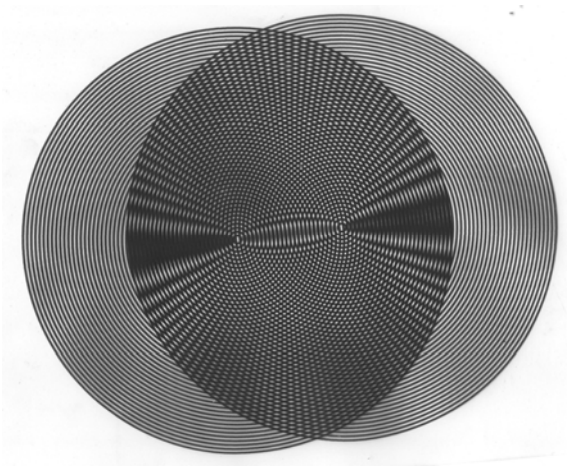

Figure 8. Moire pattern between two patterns of regular spaced rings.

Comments about the surface energies – In the analysis above we have modeled the surface interactions as if the patterned substrates are perfectly planarized. This might not be the case, and in fact is not the case in our experiments, where the Au lines are patterned onto a Pyrex substrate. These lines are 200 nm thick, and thus the Pyrex never comes into contact with either the Pyrex or Au on the opposing substrate. The interfacial energies in the exchange energy must be modified to reflect that gaps exist and that the Pyrex surfaces are actually in contact with the atmosphere. Letting the subscript A refer to Au, the interfacial energy γ_{AB} becomes $\gamma_A + \gamma_B$ the interfacial energy γ_{BB} becomes $2\gamma_B$, and the exchange energy becomes $\Delta\gamma = 2\gamma_A - \gamma_{AA}$. So the registration force is solely due to the Au interactions, or to the interactions of the ligands on the Au surfaces, as the case may be. In addition, if the Au features are rough then their surfaces will only be in partial contact, which will further reduce the observed exchange energy.

2. EXPERIMENTAL PROCEDURE

2.1. Test patterns

2.1.1. Alignment test patterns

Our test pattern is an array of lines photolithograhically deposited onto silicon and Pyrex wafers. Each die is 2 cm x 2 cm with 25 μm gold lines separated by 25 μm, as shown in Figure 9. The gold was 200 nm thick on a 20 nm thick chromium adhesion layer.

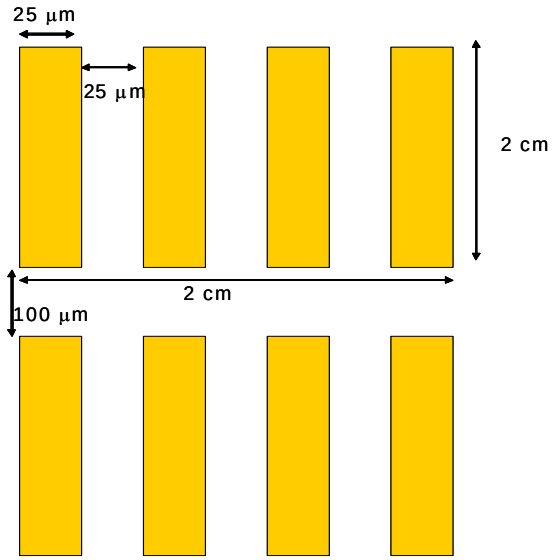

Figure 9. Array of gold lines used for alignment experiments.

2.1.2. Bonding test patterns

For Au-Au bonding experiments, arrays of circular gold pads on silicon and quartz were fabricated. These arrays are described below.

Bonding test array #1: An 8x8 array of gold balls (Fig. 10). The gold balls are wire bonded to 100 μm square gold pads and are ~25 μm tall.

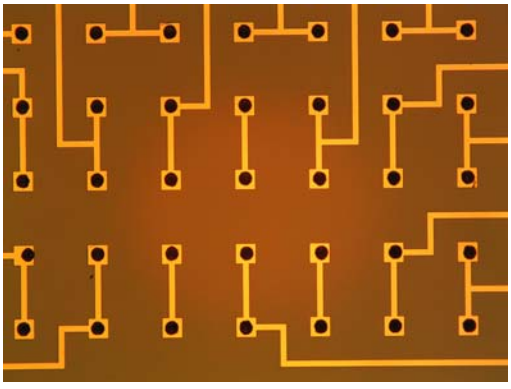

Figure 10. An optical microscope image of test array#1, gold bumps wire bonded to gold pads.

Bonding test array #2: Arrays of circular gold pads having different sizes and spacings, as shown in Fig. 11(a) were fabricated using evaporation at CINT. The arrangement of the arrays on 1 cm x 1cm squares on 4-inch silicon and quartz wafers is shown in Fig. 11(b). The gold thickness is 1 μm on a 20nm thick layer of titanium. The diameter of the pads, *d*, is 5, 10, 15, 20, or 25 μm, with spacings, *s*, that are twice the pad diameter.

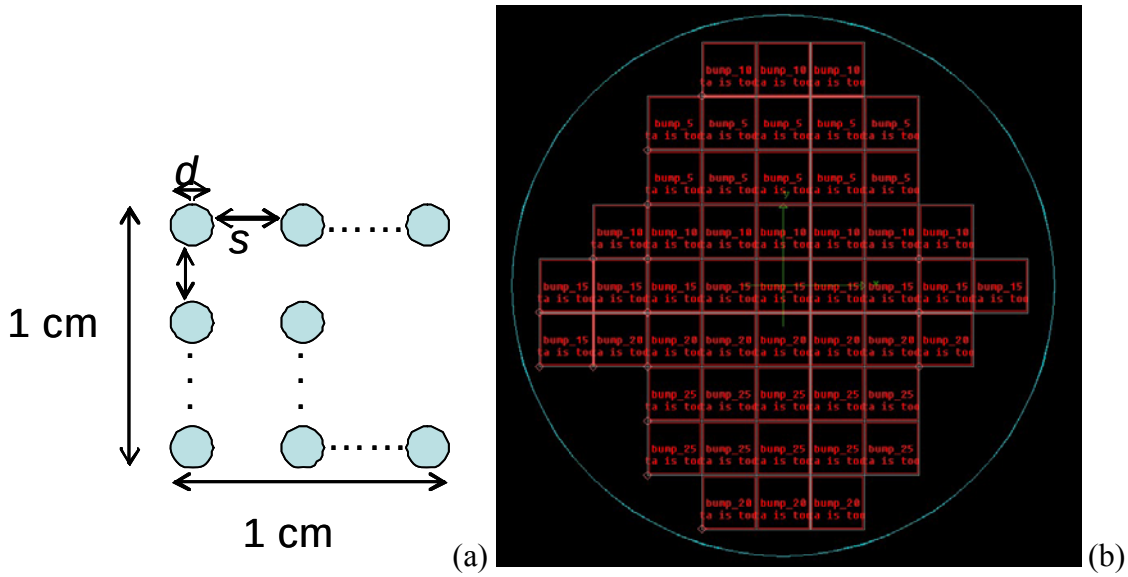

Figure 11. (a) Circular gold pads having a range of diameters and spacings were arranged on 1 cm x 1 cm squares then patterned on silicon and quartz. (b) The layout of the pad arrays on a 4-inch wafer.

Bonding test array #3: The array shown in Fig. 12 consists of hexagonal 1μm-thick aluminum-1% silicon pads that were metalized by an outside vendor, PacTech, using their electroless nickel immersion gold (ENIG) and electroless nickel, electroless palladium immersion gold (ENEPIG) processes. The thickness of the gold is 100 nm. The Ni is 5, 10, or 25 μm thick. The Pd is 5 or 25 μm thick. The pads are ~80 μm diameter on 400 μm spacings. Each die is 1cm x 1cm.

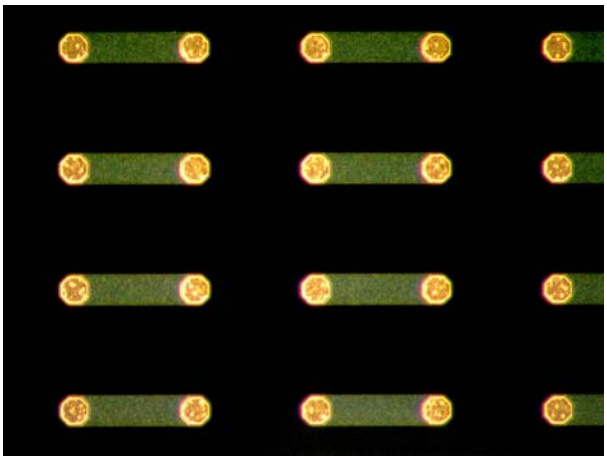

Figure 12. An optical microscope image of bonding test array #3, immersion gold bumps on nickel pads.

2.1.3. Gold surface treatment and bonding

We compared the alignment accuracy of uncoated and dodecanethiol SAM-coated gold test arrays. The uncoated arrays were cleaned in a 5:1:1 solution of deionized water, 30% H_2O_2, and H_2SO_4 for 5-7 min. The coated arrays were cleaned in the same manner, then immersed in a 1 mM solution of dodecanethiol in ethanol for ~24 h, rinsed in ethanol, and air dried.

The bonding experiments compared three surface pre-treatments, as shown in Table 1 for the #1 test arrays (gold ball arrays). The experimental matrix for the #3 test arrays (electroless Ni/Pd immersion gold pad arrays) is shown in Table 2.

Table 1. Experimental matrix for bonding studies of #1 test arrays. Gold thickness=25 μm.

# of die pairs	Solvent clean 5-7 min.	Ar plasma clean 375W, 10-15 psi 5 min.	SAM coated 1mM $C_{12}SH$ in EtOH 28 h
5	X	---	---
5	---	X	---
5	X	---	X

Table 2. Experimental matrix for bonding studies of #3 test arrays. Gold thickness=100 nm

# of die pairs	Ni/Pd Thickness (μm)	Solvent clean 5-7 min.	Ar plasma clean 375W, 10-15 psi 5 min.	SAM coated 1mM $C_{12}SH$ in EtOH 24 h
3	5	X	---	---
3	5	---	X	---
3	5	X	---	X
3	10	X	---	---
3	10	---	X	---
3	10	X	---	X
3	25	X	---	---
3	25	---	X	---
3	25	X	---	X
3	5/5	---	---	X
3	10/25	---	---	X

After the test arrays were given the appropriate surface treatment, they were immediately bonded using a Finetech Lamdba flip-chip bonder with 18-200N of force for 30s to 30 min., at 150-185°C. The bonds were sheared using a Dage 4000 shear tester which gives a pass/fail result based on Mil-Std-883F for die shear, and also gives the shear strength value.

3. RESULTS AND DISCUSSION

3.1. Experimental validation of registration

In this chapter we describe the experiments we conducted to demonstrate that patterned features can lead to high resolution registration, in fact, far better than can be produced by our aligner. Our first experiments utilized 2 cm square substrates patterned with 25 micron Au lines on 50 micron centers, so that the gaps between the lines are 25 microns. These Au lines stand above the substrate by ~220 nm- 200 nm of Au on 20 nm of Cr, and thus only the Au lines on opposing dies can come into contact, unless the two die come together out of registration, which did not occur. The Au surfaces were left either bare or were coated with dodecanethiol, applied as an ethanolic solution.

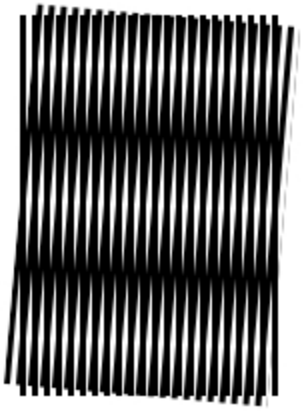

Figure 13. Moire pattern between two identical sets of equally spaced lines that are misoriented.

One die was placed on a microscope stage and the second die was placed on top, which generally produced a Moire pattern indicative of a relative misorientation, as in Figure 13. The top die was then gently prodded by hand in such a manner as to align the dies. Such a process would seem much too inaccurate to produce the desired lateral registration of the 25 micron wires (which are roughly a third the diameter of a human hair) yet we repeatedly obtained excellent registration, such as that shown in Figure 14. This alignment accuracy was better than 1 micron, which is far better than the 5 micron machine accuracy in our microfab.

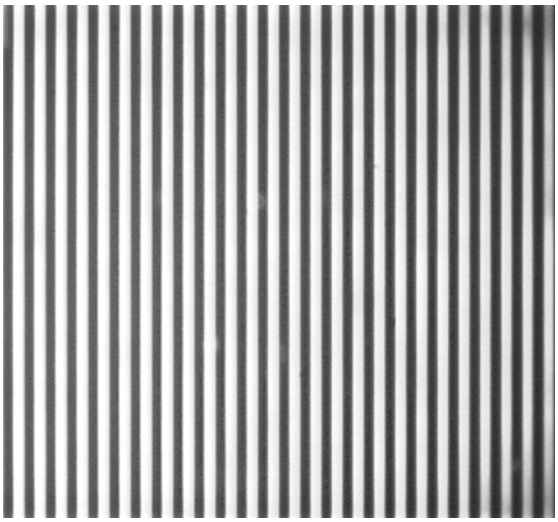

Figure 14. Essentially perfect alignment of two 2 cm square Pyrex die patterned with 25 micron Au lines spaced on 50 micron centers. This alignment was achieved manually, and is due to the surface interactions between the Au lines.

When these patterned die are placed together such that the lines are on the outer surfaces and the Pyrex surfaces are in contact, it is not possible to manually prod the upper die to achieve line alignment, which demonstrates the effectiveness of the interactions between the patterned surfaces. Alignment experiments were done with Au lines coated with self-assembled monolayers of dodecanethiol. We found that on average these die could be brought into alignment in less than half the time as for the uncoated lines. It is interesting to note that partial alignment did not generally occur: Anytime a misorientation of the die was corrected by prodding the upper die at one corner it was found that the lines were automatically brought into lateral registration, allowing imaging through the die, such as in Figure 15.

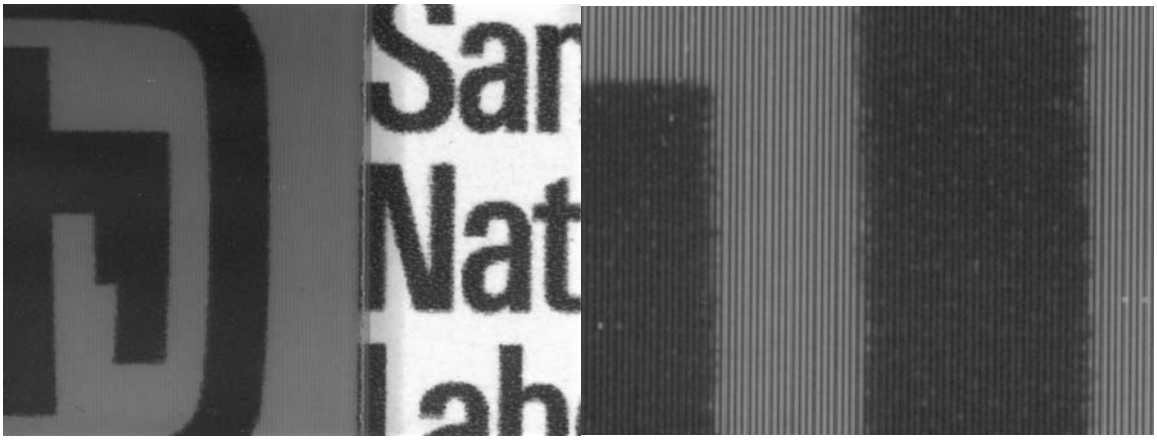

Figure 15. (left) The left-hand side of this image is covered by the die pair patterned with Au lines and brought into registration by the interactions between these lines, which were coated with self-assembled monolayers of dodecanethiol. (right) When the image is magnified, the registered lines can be clearly seen. This image includes the upper right 'shoulder' of the thunderbird.

These studies demonstrate that it is possible to use interactions between micropatterned surfaces to vastly increase alignment accuracy. As a follow-on project, it would be interesting to work with patterns that reduce the need for accurate initial placement, and that do not easily lead to misregistration, as can easily occur in patterns with translational symmetry. For example, to improve the simple, periodic line patterns we have studied one could create a periodic sinusoidal modulation in the line spacing and/or line width. If this modulation had a periodicity of ten lines, then the initial registration accuracy could be reduced by a factor of ten without fear of misregistration.

3.2. Bonding

In a real application, the aligned Au micropatterned surfaces would be permanently bonded using heat and a compressive load. Temperatures lower than 200°C are desirable to prevent thermal damage to the devices, as are minimal bonding loads to prevent cracking of thinned die/wafers. It is currently possible to bond Au to Au at 150^{o}C or less under moderate loads provided the Au surfaces are Argon plasma cleaned [10,11,14,15]. Even more impressive results can be achieved if the surfaces are ultra-planar: room temperature bonding in 60 h without any load [16]! The RMS surface roughness of the wafers used in these studies was 1-3 Å. In the absence of comparable planarization capabilities at SNL, we did not attempt to reproduce these results, so we focused on achieving bonds at ~150^{o}C, which is still quite reasonable.

In this section we present the results of bonding experiments performed on the bonding test arrays described in the Experimental Procedure section. These arrays were designed to study bonding of Au features having a range of thicknesses and that were deposited using three standard processes that are likely to be used in SNL applications. The deposition processes are: 1. Au ball bonding; 2. Evaporation; and 3. Electroless nickel immersion gold (ENIG).

Test array #1 - In Table I we list the bonding conditions, surface preparations, and shear strengths for the #1 test arrays. These arrays have Au ball bonds ~25 μm tall. All arrays were bonded at temperatures from 150-165°C and passed the shear test if the shear strength was at least 1 kg. Most of the bonds fail at the Au-Au interface; others fail due to debonding of the underlying Cr adhesion layer from the silicon. These results agree with those reported by others for Au stud bumps [10,14] and electroplated bumps [11].

Table 3. Au-Au bonding conditions, surface preparation, and shear strength for gold bump arrays. Bump height=25 μm.

Plasma (Ar)	Force (N)	Temperature (^{o}C)	Duration (seconds)	Shear strength (kg)	Surface preparation
none	18	155	30	0.552	5 min dilute piranha, 28 hr dodecanethiol
none	18	150	40	1.171	5 min dilute piranha, 28 hr dodecanethiol
none	20	150	40	1.402	5 min dilute piranha, 28 hr dodecanethiol
none	20	150	40	1.414	5 min dilute piranha, 28 hr dodecanethiol
none	20	150	45	1.523	5 min dilute piranha, 28 hr dodecanethiol
5 min.	20	150	45	0.934	none
5 min.	20	155	45	1.231	none
5 min.	20	165	45	1.173	none
5 min.	20	155	45	1.12	none
5 min.	20	150	45	1.463	none
none	20	150	45	1.553	5 min dilute piranha
none	20	150	45	1.075	5 min dilute piranha
none	20	155	45	1.504	5 min dilute piranha
none	20	150	40	0.971	5 min dilute piranha
none	20	150	40	0.687	5 min dilute piranha

Test array #2 – The test arrays fabricated at CINT using evaporation were not suitable for bonding experiments because of poor adhesion of the Au-Ti: Each die had regions where the Au and the Ti adhesion layer had completely debonded from the silicon and quartz wafers.

Test array #3 – These test arrays have only 100 nm of Au, which is thinner than that used in most other studies. (The Au was only 20 nm thick in the room temperature bonding study we mentioned previously, but the surfaces had a RMS surface roughness of 1-3 Å.) We found that the minimum temperature at which these arrays bonded is 165°C. These bonds required higher loads (200N) and longer times (30 min.) to form than did the #1 test arrays. The only samples that bonded were those having a dodecanethiol SAMs coating (see Table 4). The shear strength of these bonds (0.067kg) is not yet up to Mil-Std-883F requirements, but the bonding process is not yet optimized. When the temperature was increased to 185°C, bonds formed having shear strengths of 0.149-0.235kg. As indicated in Table 4, bonding for 10 min. at 165°C produced temporary bonds that held together anywhere from a few hours to a few days. Temporary bonds that are electrically continuous enable the pre-testing of devices before they are irreversibly attached to costly assemblies, thus eliminating waste and production delays.

Table 4. Effect of applied load, bonding time, and surface treatment on the bondability of immersion gold pad arrays at 165°C and 185°C. Au thickness=100 nm.

		Surface treatment and bondability		
Force (N)	Time	Dilute piranha	Ar plasma	Dilute piranha Dodecanethiol
20	45 sec	*Did not bond*	*Did not bond*	*Did not bond*
20	60 sec	*Did not bond*	*Did not bond*	*Did not bond*
200	10 min	*Did not bond*	*Did not bond*	Temporary bond
200	30 min	*Did not bond*	*Did not bond*	Bonded
200	30 min/185°C	---	*Did not bond*	Bonded

The Au-Au bonding studies demonstrate that the dodecanethiol SAMs do not interfere with and may actually enhance the bondability of Au micropatterned surfaces. In fact, 100 nm thick immersion Au films bonded only when they were coated with dodecanethiol SAMs. The 100 nm Au films required slightly higher temperatures to bond (165-185°C) and higher loads (200N) than those used for Au bump bonding. We have not found any reports of Au-Au bonding of such thin Au layers.

4. CONCLUSIONS

This late-start LDRD demonstrates that it is possible to use interactions between micropatterned surfaces to vastly increase alignment accuracy. The key outcomes of this project are listed below.

1. Submicron alignment of dies having micropatterned commensurate gold features that have been functionalized with alkanethiol ligands before the die are brought into contact has been achieved. The ligand interfacial energy is minimized when the features on the die are brought into registration, due to favorable interactions between the complementary ligand tails.

2. We have computed the alignment forces and torque between two surfaces patterned with arrays of lines or square pads to illustrate how best to maximize the tendency to align.

3. We have studied complex, aperiodic patterns such as rectilinear pad assemblies, concentric circles, and spirals that point the way towards extremely precise alignment.

4. An array of lines with a sinusoidal modulation in their spacing is an approach that could greatly reduce the need for precision placement, while still retaining the high registration force given by fine lines.

5. After alignment is achieved, standard bonding techniques can be used to create precision permanent bonds. We have demonstrated Au-Au bonding of dodecanethiol SAM-coated Au features at 150-185°C. The SAM-coated and Ar-plasma treated Au bumps bond under the same conditions and have comparable shear strengths. The Au thin films are more difficult to bond. In fact, only the SAM-coated Au films bonded.

6. It may be possible to tune the bonding conditions to create temporary bonds and thus enable pre-testing of devices before they are irreversibly attached to a substrate.

7. The alignment and bonding process developed in this LDRD is applicable to many SNL applications.

5. REFERENCES

1. U. Srinivasan, D. Liepmann, R.T. Howe, "Microstructure to substrate self-assembly using capillary forces," *J. Microelectromech. Sys*., **10** [1], 17-24 (2001).

2. B.R. Martin, D.C. Furnange, T.N. Jackson, T.E. Mallouk, T.S. Mayer, "Self-alignment of patterned wafers using capillary forces at a water-air interface," *Adv. Funct. Mater*., **11** [5], 381-386 (2001).

3. X. Xiong, Y. Hanein, J. Fang, Y. Wang, W. Wang, D.T. Schwartz, K.F. Bohringer, "Controlled multibatch self-assembly of microdevices," *J. Microelectromech. Sys*., **12** [2], 117-127 (2003).

4. M.R. Tupek, K.T. Turner, "Submicron aligned wafer bonding via capillary forces," *J. Vac. Sci. Technol. B*., **25** [6], 1976-1981 (2007).

5. J. Dalin, J. Wilde, A. Zulfiqar, P. Lazarou, A. Synodinos, N. Aspragathos, "Electrostatic attraction and surface-tension driven forces for accurate self-assembly of microparts," *Microelectronic Engineering*, **87**, 159-162 (2010).

6. T. Fukushima, E. Iwata, T. Konno, J.-C. Bea, K.-W. Lee, T. Tanaka, M. Koyanagi, "Surface tension-driven chip self-assembly with load-free hydrogen fluoride-assisted direct bonding at room temperature for three-dimensional integrated circuits," *Appl. Phys. Lett*., **96**, 154105(1-3) (2010).

7. J-M. Kim, K. Yasuda, K. Fujimoto, "Resin self-alignment processes for self-assembly systems," *J. Electron. Packag*., **127**, 18-24 (2005).

8. A.H. Slocum, A.C. Weber, "Precision passive mechanical alignment of wafer," *J. Microelectromech. Sys*., **12** [6], 826-834 (2003).

9. J. Huang, D.A. Dahlgren, J.C. Hemminger, "Photopatterning of self-assembled alkanethiolate monolayers on gold: A simple monolayer photoresist utilizing aqueous chemistry," *Langmuir*, **10**, 626-628 (1994).

10. X.F. Ang, F.Y. Li, W.L. Tan, Z. Chen, C.C. Wong, "Self-assembled monolayers for reduced temperature direct metal thermocompression bonding," *Appl. Phys. Lett.*, **91**, 061913(1)-061913(3) (2007).

11. L.C. Chin, X.F. Ang, J. Wei, Z. Chen, C.C. Wong, "Enhancing direct metal bonding with self-assembled monolayers," *Thin Solid Films*, **504**, 367-370 (2006).

12. C.M. Whelan, M. Kinsella, L. Carbonell, H.M. Ho, K. Maex, "Corrosion inhibition by self-assembled monolayers for enhanced wire bonding on Cu surfaces," *Micro. Engr*., **70**, 551-557 (2003).

13. T. Laiho, J.A. Leiro, "Influence of initial oxygen on the formation of thiol layers," *Appl. Surf. Sci*., **252**, 6304-6312 (2006).

14. E. Higurashi, D. Chino, T. Suga, R. Sawada, "Au-Au surface-activated bonding and its application to optical microsensors with 3-D structure," *IEEE J. Sel. Top. Quant. Electron*., **15** [5], 1500-1505 (2009).

15. E. Higurashi, T. Imamura, T. Suga, R. Sawada, "Low-temperature bonding of laser diode chips on silicon substrates using plasma activation of Au films," *IEEE Phot. Technol. Lett*., **19** [24], 1994-1996 (2007).

16. Q. –Y. Tong, "Room temperature direct metal bonding," *Appl. Phys. Lett*., **89**, 182101(1)-182101(3) (2006).

DISTRIBUTION

1	MS1084	Catalina Ahlers	01746-1
1	MS0352	Dahwey Chu	01715
1	MS0352	Kevin Ewsuk	01715
1	MS1078	Wahid Hermina	01710
1	MS1074	Dale Hetherington	01746
1	MS1415	James Martin	01112
1	MS1415	Diane Peebles	01112
1	MS0892	Lauren Rohwer	01715
1	MS1082	W. Kent Schubert	01717
1	MS1077	Thomas Zipperian	01740
1	MS0899	Technical Library	9536 (electronic copy)
1	MS0359	D. Chavez, LDRD Office	01911


Sandia National Laboratories